Climate Dynamics (2020) 55:1685–1696
https://doi.org/10.1007/s00382-020-05420-1

Recent changes in heatwave characteristics over Korea

Donghyuck Yoon[1] · Dong-Hyun Cha[1] · Myong-In Lee[1] · Ki-Hong Min[2] · Joowan Kim[3] · Sang-Yoon Jun[4] · Yonghan Choi[4]

Received: 25 November 2019 / Accepted: 5 June 2020 / Published online: 14 August 2020

Abstract
Global warming and abnormal climate change have resulted in an increase in the frequency of severe heatwave events. Recently, a series of extreme heatwave events have occurred in South Korea, and the damage from these events has also been increasing. Thus, it is necessary to analyze the mechanisms for generating and developing heatwaves. In this study, the long-term trend for heatwave events in South Korea was investigated using cluster analysis. Heatwave events in a 38-year period in South Korea were defined, and their synoptic patterns were categorized into three clusters. The number of heatwave days of cluster 2, which is related to the anomalous positive geopotential height (GPH) over the Kamchatka Peninsula, was found to significantly increase in recent years (2000–2018) compared with the past (1981–1999). In contrast, the frequency of cluster 3 associated with a negative GPH anomaly over the Kamchatka Peninsula decreased in the same period. There were five regions, including northern China and the Kamchatka Peninsula, where the mid-level GPH significantly increased between 2000 and 2018. This change in GPH was positively (negatively) correlated with the patterns associated to long-term variability of heatwave days of cluster 2 (cluster 3). The long-term trends of the GPH anomalies over five regions showed a significant correlation with the North Atlantic Oscillation (NAO) index during midsummer. As a result, it is likely that the heatwave events related to cluster 2 (cluster 3) have increased (decreased) in South Korea because the long-term variability of the summer NAO has recently induced a favorable (unfavorable) atmospheric condition for cluster 2 (cluster 3).

Keywords Heat wave · Cluster analysis · Long-term variability · North Atlantic Oscillation · South Korea

1 Introduction

Recently, numerous severe heatwave events have caused global socioeconomic damage (Luterbacher et al. 2004; Barriopedro et al. 2011; Coumou et al. 2013). Previous studies have noted that the frequency of heatwaves and their damage has increased because of global climate change (Meehl and Tebaldi 2004; IPCC 2013). In recent summers, East Asia, including Eastern China, Japan, and the Korean Peninsula, has most been severely inflicted by heatwaves (Nakai et al. 1999; Kysely and Kim 2009; Sun et al. 2014; Hu and Huang 2020).

In this research, we investigate the multi-decadal characteristics of heatwaves, focusing on South Korea. A representative heatwave event over South Korea occurred in the summer of 1994 when the highest maximum daytime temperature was recorded as 39.4 °C, resulting in more than 3000 heat-related victims (Kysely and Kim 2009; Min et al. 2019). Since 1994, a series of extreme heatwave events occurred in South Korea, causing widespread damage (e.g., August 2013, August 2016, July–August 2018). In the past, the mechanism of heatwaves in South Korea was not well understood. However, there are now extensive studies on the topic with the recent increase in severe heatwave events (Lee and Lee 2016; Yeh et al. 2018; Yoon et al. 2018; Kim et al. 2019; Yeo et al. 2019; Min et al. 2019). In particular, Lee and Lee (2016) examined the decadal change in the

✉ Dong-Hyun Cha
dhcha@unist.ac.kr

[1] School of Urban and Environmental Engineering, Ulsan National Institute of Science and Technology, Ulsan 44919, Republic of Korea

[2] Department of Astronomy and Atmospheric Sciences, Kyungpook National University, Daegu 41566, Republic of Korea

[3] Department of Atmospheric Science, Kongju National University, Gongju, Republic of Korea

[4] Unit of Arctic Sea-Ice Prediction, Korea Polar Research Institute, Incheon 21990, Republic of Korea

relationship between heatwave frequency in Korea and large-scale atmospheric patterns. They suggested that the relationship between heatwaves over Korea and tropical forcing tends to be weakened. At the same time, the influence from the Arctic is enhanced, representing the correlation between heatwave days (HWDs) and the summertime Arctic Oscillation index (Thompson and Wallace 1998). Yeh et al. (2018) investigated the characteristics of heatwave events in August 2016. They mentioned that the intensity of the geopotential height (GPH) over the Kamchatka Peninsula in August 2016 was the strongest since 1979; it acted as an atmospheric block in the downstream region of the Korean Peninsula. They also identified that a zonal wave train, related to the circumglobal teleconnection pattern, may have contributed to the heatwave over South Korea in August 2016. Similarly, some studies have shed light on the characteristics of the circulation and teleconnection patterns associated with the heatwaves in South Korea. However, the above studies have limitations in that they either composite all heatwave events to generalize the characteristics (Lee and Lee 2016; Kim et al. 2019) or analyze only several heatwave cases (Yeh et al. 2018; Min et al. 2019).

Yoon et al. (2018) suggested that the spatial distributions of the maximum surface air temperature in South Korea between 1981 and 2016 may be categorized into three groups using a cluster analysis method. They also assigned different synoptic characteristics in terms of the 500 hPa geopotential height. Yeo et al. (2019) classified heatwaves in South Korea into two distinct types based on the spatial patterns of the large-scale atmospheric circulation anomalies; the zonal wave (Z-wave) type and meridional wave (M-wave) type. They postulated that the circulation patterns of the Z-wave were closely related to the positive summer North Atlantic Oscillation (NAO) signal (Folland et al. 2009). However, the atmospheric patterns of the Z-wave type heatwave suggested by Yeo et al. (2019), were not representative of the heatwave events caused by Kamchatka blocking, such as in August 2016.

The relationship between HWDs in China and the summer NAO index was investigated by Deng et al. (2019). They reported that the correlation coefficient relating the decadal variation of the HWDs in the Yangtze River valley and summer NAO index between 1961 and 2015 was 0.4, exceeding the 95% confidence level. They also emphasized the effect of sea surface temperature (SST) over the tropical North Atlantic Ocean on HWDs in China. They suggested that HWDs in northern China have a significant relationship with the warm SST anomaly in the tropical North Atlantic Ocean, resulting in the generation of Rossby wave trains propagating eastward and inducing an intensified anticyclone over northern China. Lim and Seo (2019) revealed that the SST anomaly over the North Atlantic Ocean can be a predictor for forecasting extreme summer temperatures in South Korea. They suggested that the tripolar pattern of the North Atlantic Ocean SST anomaly, related to heatwave events in South Korea, is similar with the negative phase of the summertime NAO. Jian-Qi (2012) also demonstrated that the summer NAO was closely related to the extreme hot events in northern China, with the negative-phase summer NAO corresponding to greater HWDs in that region. The results of previous studies suggest that the activity of the summer NAO could be an important parameter for HWDs in East Asia.

The results of previous studies suggest that the atmospheric pattern of heatwave events in Korea can be classified into several types with distinct large-scale patterns, and HWDs may have a long-term variability associated with climate index, especially NAO. In this study, we define heatwave events and categorize the synoptic patterns of the heatwave events in South Korea using the cluster analysis method. Then, the long-term variabilities of HWDs are investigated for three clusters. Finally, the relationship between the long-term variabilities of the large-scale trends and heatwaves in South Korea and summer NAO is analyzed. The data and methods used in this research are described in Sect. 2. Section 3 presents the detailed results and interpretation. The summary and discussion are provided in Sect. 4.

2 Data and methods

2.1 Data

The daily maximum surface air temperature (hereafter, TMAX) data from the automated surface observing systems (ASOSs) of 98 stations of the Korea Meteorological Administration (KMA) were used to define heatwave events in South Korea for a period of 38 years (1981–2018). Temporal mean atmospheric conditions for heatwave clusters, such as GPH and its anomaly, were represented using 6 hourly ERA-interim reanalysis (ERAIN) data (Dee et al. 2011) from 1981 to 2018. The 6 hourly ERAIN data were converted to daily data for the analysis. A GPH anomaly was calculated by subtracting 38 years climatological mean fields. TMAX anomalies were determined for each HWD by subtracting a 38 years climatological mean TMAX, demonstrated by using the daily ASOS data from 1981 to 2018. The daily NAO index was obtained from the Climate Prediction Center (https://www.cpc.ncep.noaa.gov) to investigate the relationship between the summer NAO (from July 11 to August 20) and heatwave events in South Korea.

2.2 Heat wave definitions and cluster analysis

Although a heatwave events can be interpreted as a period of abnormally, uncomfortably hot and unusually humid weather (Ward 1925), in this study, they are identified considering only TMAX. The procedure for defining heatwave events, which includes determining the criteria values and the method for cluster analysis, mainly follows a previous study (Yoon et al. 2018). The heatwave events in South Korea between 1981 and 2018 were defined by considering three spatiotemporal criteria: temperature threshold, spatial continuity, and temporal continuity.

First, daily "hot" stations are defined when TMAX in the KMA ASOS station data exceeds the temperature threshold value (T, 33 °C in this study); the official KMA criteria for a heatwave warning. All 98 station TMAX data between 1981 and 2018 were filtered by comparisons with the threshold value, T. Then, the isolated hot stations were eliminated if a given station whose ratio of the total number of stations (N) to the number of hot stations (n) within a given distance (D, 0.75° in this study) was smaller than a specific value (α) (Eq. 1). Isolated stations were then eliminated to obtain the spatial continuity of heatwave events for each time step:

$$\frac{n}{N} \leq \alpha \tag{1}$$

Yoon et al. (2018) used 0.4 as the α value for spatial continuity as Ren et al. (2012) suggested that it should be in the range 0.3–0.5. In this study, the threshold value α was increased to 0.6. This was done because, first, HWDs filtered by 0.4 of α have been overestimated compared with those reported by KMA, which calculates HWDs using the same observation data without the spatial continuity criterion. Second, it is necessary to select the α, taking into account the density of observing stations. Wang et al. (2017) used 0.4 for the threshold value because a larger α (greater than 0.5) sharply reduce the number of heatwaves in the regions where the observing stations are sparse such as in Northwestern China. However, the density of the surface stations in South Korea is much higher, and they are homogeneously located compared with those in Northwestern China. Finally, Stefanon et al. (2012) adapted a threshold of 0.6 for heatwaves in Europe and the Mediterranean region, providing reasonable results for relatively dense surface observations. We investigated the sensitivity of total HWDs to alpha values and concluded that 0.6 is the most reasonable threshold value for this study.

The spatial spread of hot stations should overlap in a single heatwave event lasting consecutive days. In other words, there should be no temporal gap between HWDs when defining a heatwave event (Stefanon et al. 2012). Thus, the ratio of overlapping hot stations between 2 days was calculated if the similarity ratio between the 2 days exceeded a specific threshold value (S, 30% in this study). This period is considered a single heatwave event, and its duration is determined as the number of HWDs.

The identified heatwave events were then classified based on the 500 hPa GPH anomaly over East Asia and North Pacific (0–70° N, 80–230° E). These anomalies were used as a criterion of clustering because they are widely recognized as distinct variables that are closely related to the synoptic characteristics of heatwaves (Meehl and Tebaldi 2004; Fischer et al. 2007; Ding et al. 2010). Similar to Yoon et al. (2018), the K-means clustering algorithm (Hartigan and Wong 1979) and Krzanowski–Lai (KL) index (Krzanowski and Lai 1988) were adapted for cluster analysis and validations. Cluster analysis is an algorithm that finds the optimized solution for the global objective function, maximizing the cohesion within a cluster. The cohesion can be statistically represented by the sum of squares (SSW) within groups. If there is no significant difference in SSW with an increase in the number of clusters (M), no additional clusters are required. Since the number of clusters (M) is sensitive to the objects (in this case, the averaged GPH anomaly in each cluster), the "elbow method" was traditionally utilized to determine the optimal number of clusters. Krzanowski and Lai (1988) created an index using the SSW in group to quantify this method, and then the KL index was defined using as follows:

$$\text{Krzanowski} - \text{Lai index}\left(\text{KL}_M\right) = \frac{\left|\text{diff}_M\right|}{\left|\text{diff}_{M+1}\right|} \tag{2}$$

$$\text{diff}_M = (M-1)^{2/D}\text{SSW}_{M-1} - M^{2/D}\text{SSW}_M \tag{3}$$

where D is the number of datasets (in this case, a total number of heatwave events). The number of clusters M that maximizes the KL index is used as the optimal cluster number K.

3 Results

3.1 Recent changes in heatwave characteristics

Throughout the heatwave definition procedure, 97 heatwave events in South Korea, with a total duration of 358 days, were identified over the 38 year period (1981–2018). The synoptic characteristics of heatwave events were categorized into three clusters using the K-means cluster analysis method. The number of clusters were determined using the KL index; K = 3 was found to be the most appropriate number of clusters for the K-means cluster analysis. Based on the cluster analysis, all 97 heatwave events were divided into 31, 26, and 40 events with HWDs of 117, 96, and 145 days, respectively. Figure 1 describes the composited

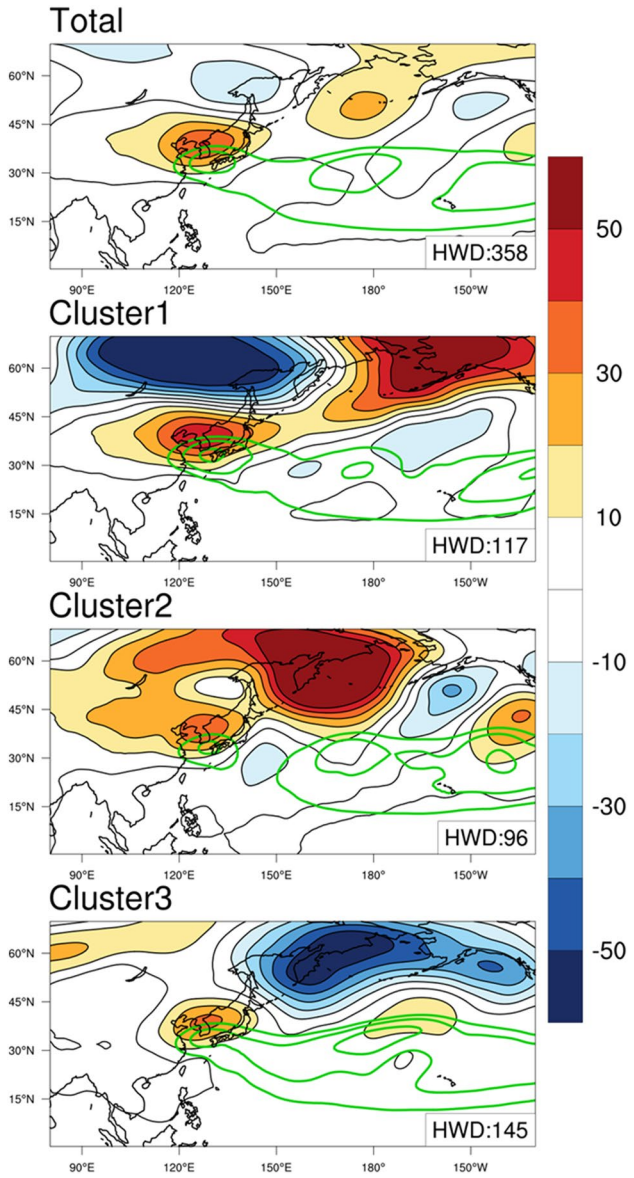

Fig. 1 Spatial patterns of the 500 hPa geopotential height anomaly [gpm] for all heatwave events and three clusters. The green colored contours demonstrate the 5870–5890 gpm geopotential height. Values in the right bottom box indicate the total HWDs for all events and each cluster

of the 500 hPa GPH anomaly for all heatwave events and three clusters. In the composite of all heatwave events, the 500 hPa GPH anomaly showed a positive maximum in the Korean Peninsula, whose pattern zonally extends. This spatial pattern coincides with the results of previous studies that have demonstrated that this is the leading synoptic pattern for heatwaves in South Korea (Lee and Lee 2016; Kim et al. 2019). In cluster 1, there was a large and strong expansion of the western North Pacific subtropical high (WNPSH) represented by the GPH at 5870–5890 gpm (green contour lines in Fig. 1) with a substantial positive GPH anomaly in the Korean Peninsula. This induces significant and extensive periods of heatwave events by south-westerly winds (e.g., summer 2018) (Li et al. 2019; Min et al. 2020). Additionally, there were negative anomalies in Siberia and large anticyclone anomalies in Alaska. In cluster 2, there was strong blocking high in the Kamchatka Peninsula and positive anomalies in the northern China–Mongolia region. Yeh et al. (2018) identified that anomalous synoptic patterns such as high pressure systems over Mongolia, which induce warm advection by northerly wind and blocking high over the Kamchatka Peninsula, can cause extreme heatwave events in South Korea (e.g., August 2016). In this case, the continental thermal high over Mongolia and the Kamchatka blocking high have a greater effect on heatwaves over Korea than the expansion of WNPSH. In cluster 3, there were negative anomalies in the Kamchatka Peninsula and Alaska, contrary to the anticyclone pattern of cluster 2. Similar to cluster 1, the GPH of cluster 3 showed an expanded WNPSH, which can also induce extreme heatwave events in South Korea (e.g., summer 1994) despite it being weaker in magnitude.

The spatial patterns of the TMAX anomaly for all heatwave events and three clusters in South Korea are described in Fig. 2. During heatwave events, the TMAX anomaly for all HWDs generally exceeded 2 °C in most regions of South Korea. In particular, the TMAX anomaly was maximum in the southeastern region of Korea. This regional distribution of the TMAX was consistent with the results of previous studies (Lee and Lee 2016; Yoon et al. 2018). In cluster 1, the TMAX anomaly was the highest over the eastern side of South Korea. This is because the south-westerly wind induced by the expanded WNPSH (Fig. 1) resulted in warm advection, and it was further heated by the Foehn effect when crossing the high mountain range in eastern Korea (Yoon et al. 2018). Further, the hottest area had slightly shifted to the west inland region in cluster 2, because of the effects of Kamchatka blocking and the continental thermal high. In particular, the mean TMAX anomaly was + 2.9 °C, the highest among the three clusters. Cluster 3 had a relatively moderate temperature distribution because of the positive GPH anomaly weaker than that for cluster 1 (see Fig. 1a, c). The results of the cluster analysis suggest that the developed subtropical high pressure and synoptic circulation system in mid-to-high latitudes may have various effects on heatwave events in South Korea.

In terms of the annual accumulated variability in HWDs, the years with three extreme heatwave events in South Korea were classified into different clusters (i.e., cluster 1-2018, cluster 2-2016, and cluster 3-1994) (blue marks in Fig. 3). A significant increasing trend was observed with the total heatwave events at the 95% confidence level (top panel in Fig. 3). Only for cluster 2, the increasing trend of HWDs was statistically significant at the 95% confidence level. This finding is consistent with that of Lee and Lee (2016). This

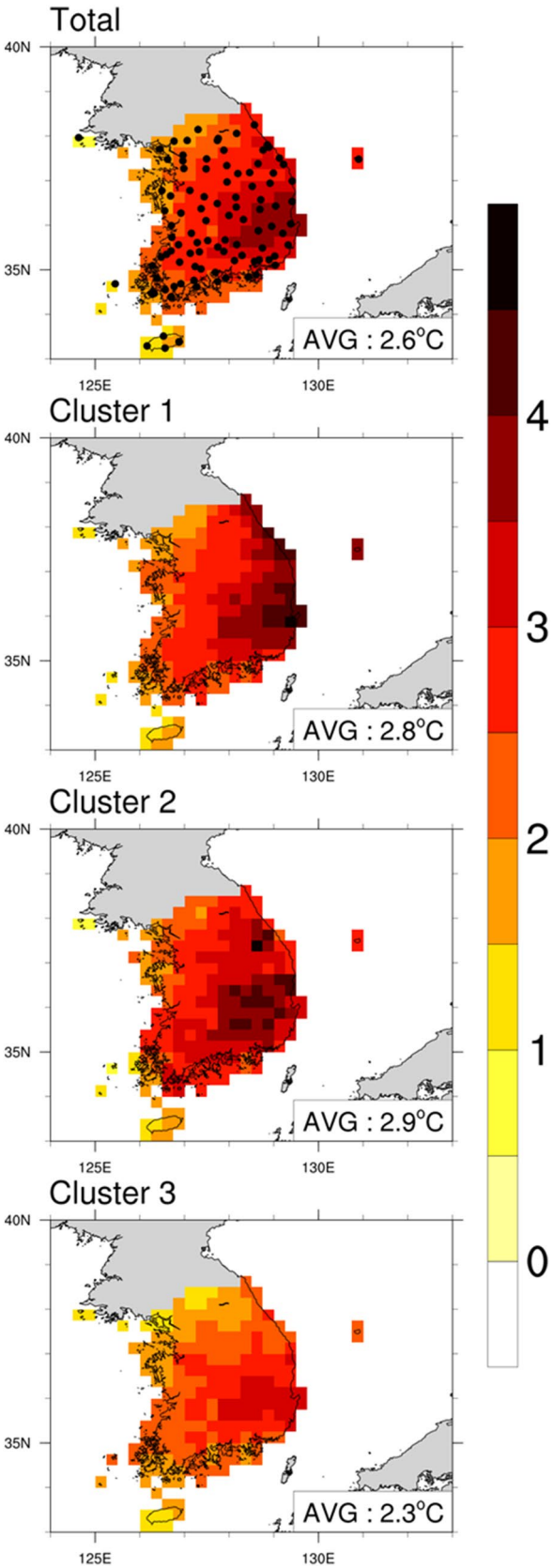

Fig. 2 Spatial patterns of the TMAX anomaly [℃] for all heatwave events and three clusters. Black dots indicate the location of Automated Surface Observing Systems over South Korea. Values in the right bottom box indicate the mean TMAX anomaly for all events and each cluster

suggests that the increasing trend of HWDs for the total heatwaves cases may be related to the heatwave events of cluster 2 rather than other clusters.

Figure 4 shows the change in HWDs between the first half (1981–1999) (hereafter, PAST) and second half (2000–2018) (hereafter, RECENT) for all clusters. HWDs of clusters 1 and 2 increased in RECENT compared with PAST, while those of cluster 3 decreased. There was no significant difference in HWDs of cluster 1 between RECENT and PAST if HWDs of 2018 were excluded. It seems that the recent increase of HWDs in cluster 1 was not associated with decadal variability. However, there was a noticeable difference in HWDs between RECENT and PAST in cluster 2 during the analysis period (Fig. 4a). The Chi-squared test showed that the HWD differences between PAST and RECENT for clusters 2 and 3 were statistically significant at the 99% confidence level; those of cluster 1 were significant at the 95% confidence level. These variations in HWDs for the PAST and RECENT were analyzed further every 10 days from June to August (Fig. 4b). We analyzed the HWD changes by dividing the days of JJA into early (1st–10th), mid (11th–20th), and late (21st–30th for June and 21st–31st for the July and August) periods. The changes in the HWDs were particularly noticeable from July 11 to August 20 for clusters 2 and 3. This period is well known for frequent and strong heatwaves in South Korea (Kim et al. 2015; Lee and Lee 2016; Yeo et al. 2019). In terms of HWDs, 90% of HWDs (322 days/358 days) occurred between July 11 and August 20. HWDs for the other periods were 36 days, which accounted for approximately 10% of all HWDs. We focused on this period to analyze the changes in HWDs. During the midsummer period (mid-July to mid-August), the changes in HWDs were 75, 17, and − 36 days for clusters 2, 1, and 3, respectively (Table 1). This implies that climatic factors may be associated with the contrasting long-term variabilities of HWDs between clusters 2 and 3.

3.2 Relationship between heatwave change over South Korea and summer NAO

In this section, the mechanism related to the difference in HWDs of PAST and RECENT for clusters 2 and 3 is presented by analyzing the long-term change in synoptic characteristics. Cluster 1 was excluded from the analysis as there was no significant long-term change in HWDs during the analysis period. To identify the large-scale pattern associated with heatwave events of clusters 2 and 3 in South Korea, the

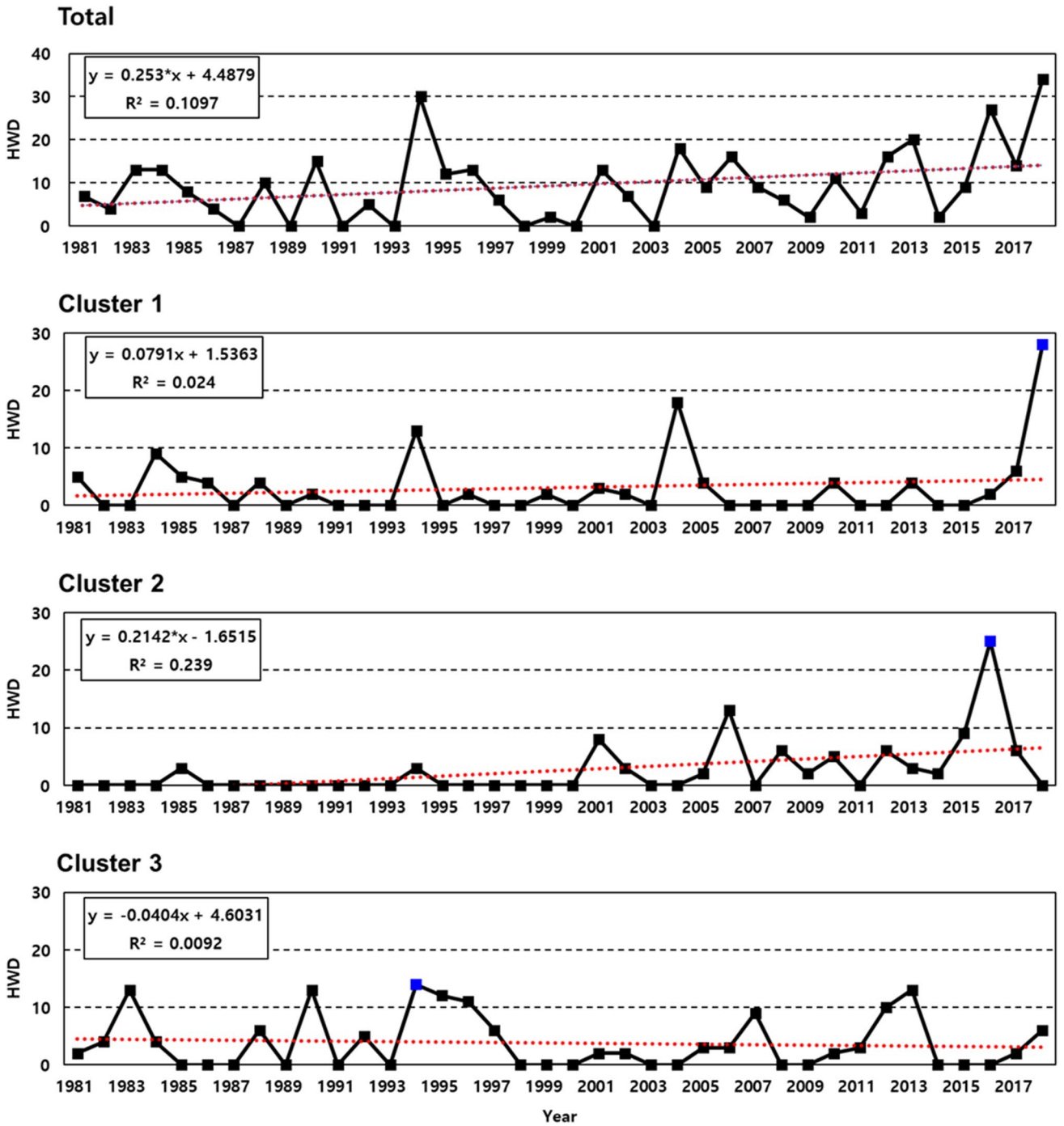

Fig. 3 Annual time series of HWDs for all heatwave events and three clusters. Red dotted lines denote the regression lines, and their statistical information are described in the left top box. The asterisk in the equation denotes that the regression coefficient is significant at the 95% confidence level. Blue marks denote 1994, 2016, and 2018, respectively

500 hPa GPH anomaly and wave activity flux (Takaya and Nakamura 2001) in the Northern Hemisphere were examined for both clusters (Fig. 5a, b). In both clusters, wave-like patterns were observed along Greenland (60–90° N, 100–0° W), eastern Europe (45–70° N, 15–65° E), northern China–Mongolia (35–55° N, 85–120° E), Kamchatka Peninsula (55–75° N, 145–170° W), and North America (40–50° N, 30–60° W), where strong GPH anomalies exist (red dashed regions in Fig. 5). These propagating features of the wavenumber-5 like pattern for two clusters coincide with the results of previous studies (Wang et al. 2013; Yeo et al. 2019; Deng et al. 2019; Kornhuber et al. 2020). It

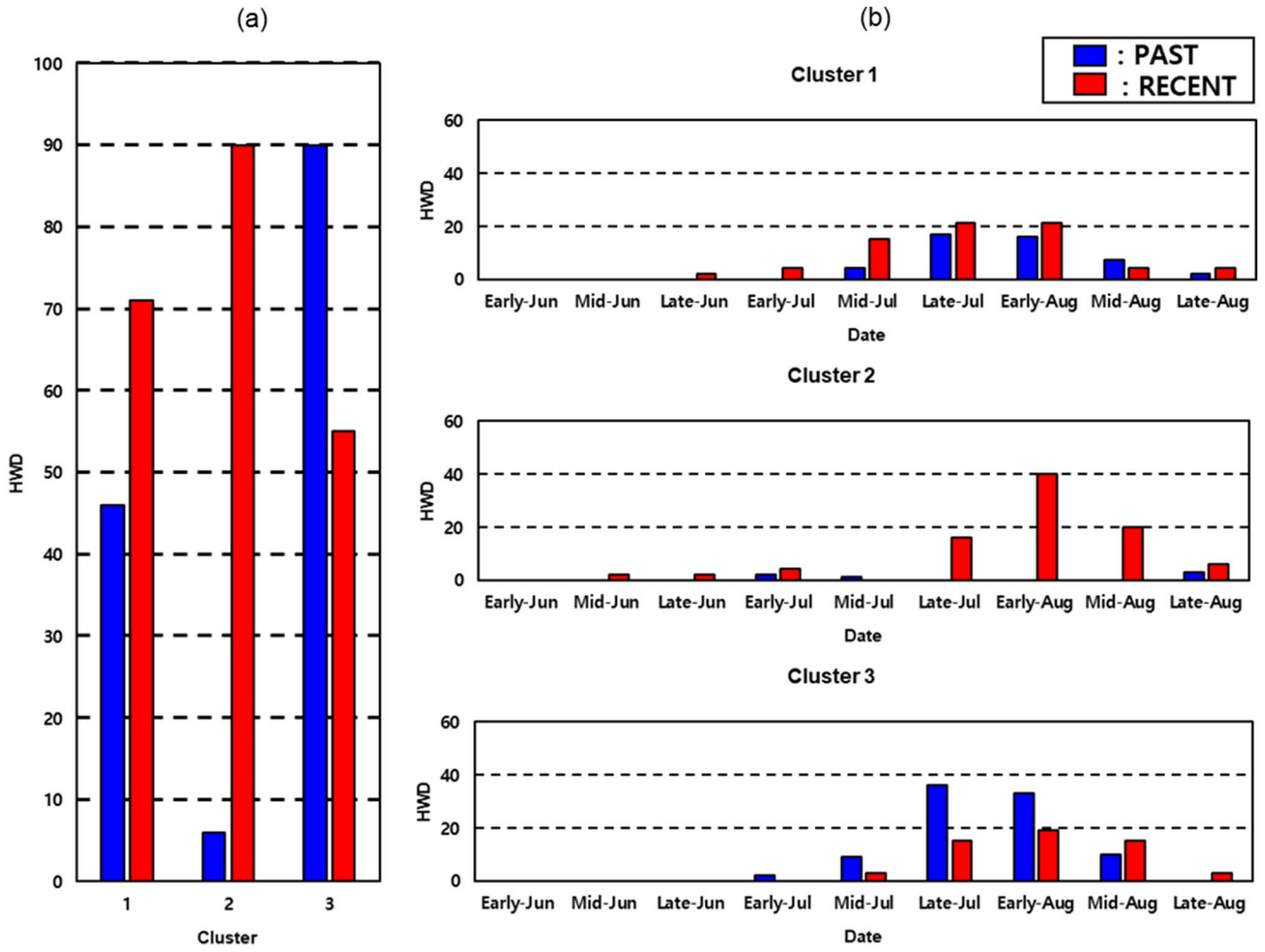

Fig. 4 **a** Total HWDs for all clusters during PAST (blue bar) and RECENT (red bar); **b** same as (**a**) but dividing every 10 days between June to August for three clusters

Table 1 Differences in HWDs between PAST and RECENT every 10 days between June to August for three clusters

Cluster	June			July			August		
	Early	Mid	Late	Early	Mid	Late	Early	Mid	Late
1	0	0	2	4	11	4	5	−3	2
2	0	2	2	2	−1	16	40	20	3
3	0	0	0	−2	−6	−21	−14	5	3

suggests that the synoptic pattern of clusters 2 and 3 may be caused by the same teleconnection mechanism, propagating from the North Atlantic Ocean to the Eurasian continent. Recent studies have shown that the mid-latitude summer circulation, with the wavenumber-5 pattern were related to extreme global events (Wang et al. 2013; Coumou et al. 2018; Kornhuber et al. 2020). Additionally, the difference in the 500 hPa GPH between the PAST and RECENT during the midsummer (Fig. 5c), which is comparable to the composite of cluster 2 (Fig. 5a), presented five regions where the positive peaks of GPH anomalies exist (red dashed boxes). The regions where the 500 hPa GPH has recently increased (Greenland, eastern Europe, northern China-Mongolia, Kamchatka Peninsula, and North America), also have positive GPH peaks in cluster 2. The pattern correlation between the 500 hPa GPH anomaly of cluster 2 (Fig. 5a) and difference in geopotential heights in RECENT and PAST (Fig. 5c) was 0.51. The large-scale distributions of the GPH anomaly of cluster 3 had an opposite signal to those of cluster 2; that is, some regions (Greenland, Kamchatka Peninsula, and North America) have negative GPH peaks. The pattern correlation between 500 hPa geopotential heights of

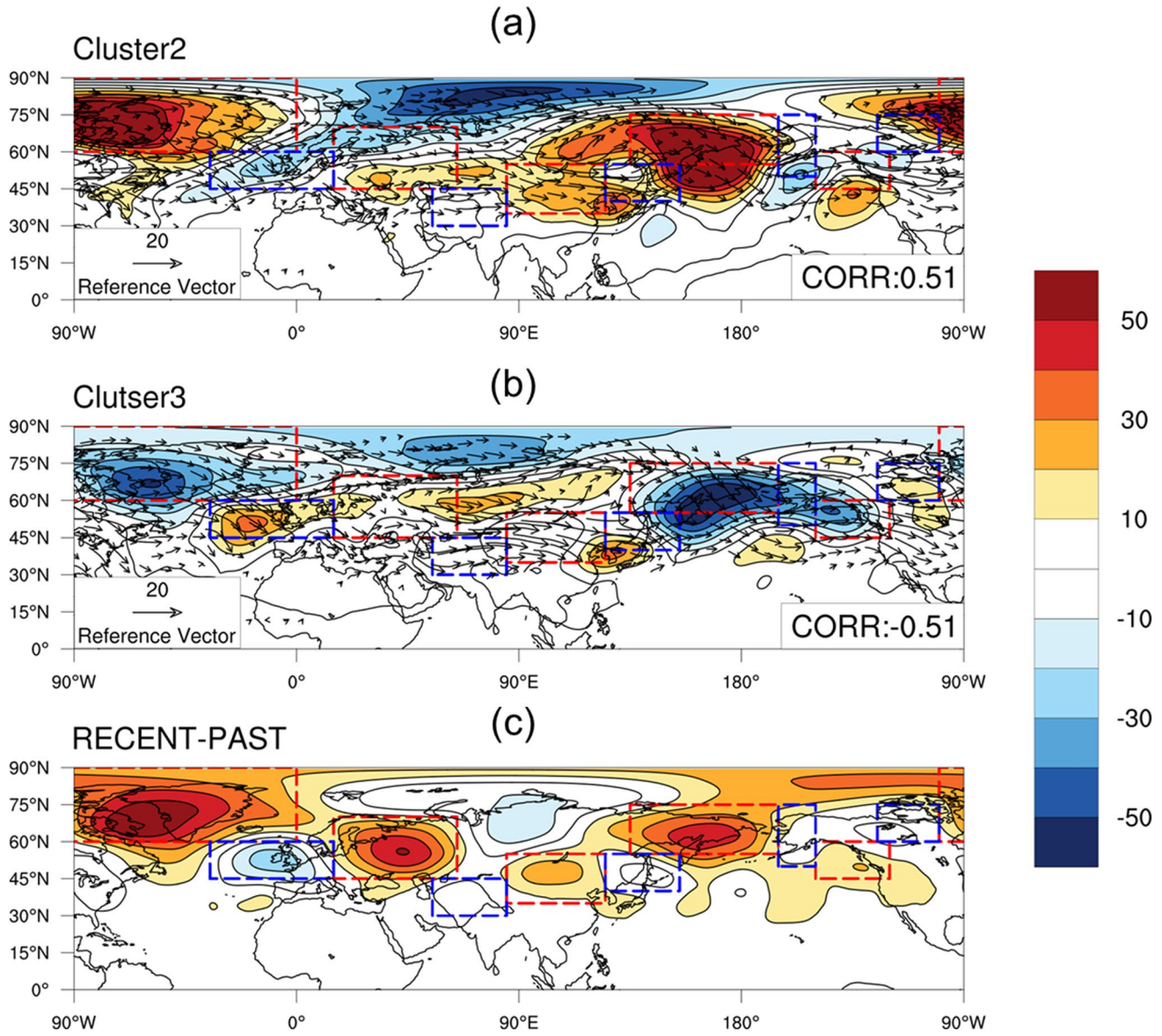

Fig. 5 Spatial patterns of the 500 hPa geopotential height anomaly [gpm] **a** for cluster 2; and **b** cluster 3 with 500 hPa wave activity flux [m^2 s^{-2}] (arrow); and **c** difference between PAST and RECENT during the midsummer (mid- July to mid-August). Values in the right bottom box of (**a**) and (**b**) indicate the pattern correlation of the 500 hPa geopotential heights with (**c**). Rectangles with red dashed lines represent the areas in which the 500 hPa geopotential height had significantly increased in (**c**). The area with decreasing 500 hPa geopotential height between the red dashed regions is marked with a blue dashed line

cluster 3 (Fig. 5b) and the difference in geopotential heights of RECENT and PAST (Fig. 5c) was − 0.51. As such, the decadal variabilities of HWDs during midsummer (mid-July to mid-August) of two clusters (cluster 2 and cluster 3) may be associated with the long-term changes in large-scale patterns. In particular, the enhancement of anticyclonic circulation in the five regions implies that the atmospheric pattern in the Northern Hemisphere has been changing in favor of cluster 2, and against cluster 3.

To better understand the change in large-scale patterns, we analyzed the relationship between these patterns and the NAO index. Recent studies suggest a potential relation between summer NAO and heatwaves over East Asia, particularly for those forced by large-scale wave patterns. The 38-year variability of the wave train during the midsummer (mid-July to mid-August) was determined by the difference in area-averaged 500 hPa GPHs between the five decreasing regions (blue dashed boxes) and increasing regions (red dashed boxes in Fig. 5). To extract long-term variability, an 8 year low-pass filter (Choi et al. 2013, 2020) was applied for the wave train and NAO indices. The long-term variations of the wave train (hereafter WAV) and summer NAO

indices (hereafter SNAO) were then compared for 38 years (Fig. 6). According to Fig. 5c, the WAV increased with some fluctuations between 1981 and 2018. In contrast, the SNAO simultaneously decreased with a temporal correlation coefficient between the WAV and SNAO of − 0.69 with a 99% significance level (Table 2). Namely, the decadal amplification of the wave train over the five regions in Fig. 5c was significantly associated with the decreasing summer NAO index. Furthermore, the temporal correlation coefficients between HWDs for clusters 2 and 3 (Fig. 3) and the SNAO (black bars in Fig. 6) during the 38 years were − 0.52 and 0.30, respectively (Table 2).

Figure 7 shows the spatial distribution of the temporal correlation coefficient between the 8-year low-pass filtered 500 hPa GPH and SNAO during the midsummer (mid-July to mid-August). Figure 7 demonstrates that the temporal correlation between the 500 hPa GPH and the SNAO had significantly negative values at the 99% confidence level in the five regions. Further, the GPH forced by NAO had a zonal wavenumber-5 pattern, beginning from the North Atlantic Ocean. These results imply that the synoptic conditions of cluster 2 (i.e., Kamchatka blocking and the continental thermal high) were affected by a teleconnection mechanism propagating from the North Atlantic Ocean to the Eurasian continent, where the decreasing summer NAO index leads to increasing 500 hPa GPH anomalies over East Asia and the Kamchatka Peninsula. This change in GPH anomalies relating to the summer NAO index tends to be unfavorable to the composite of synoptic conditions for cluster 3. This zonal wave teleconnection mechanism related to the recent developments of large-scale anticyclones caused by the decreasing trend of the summer NAO index may lead to increasing (decreasing) HWDs of cluster 2 (cluster 3) in South Korea.

Table 2 Temporal correlation coefficients among the SNAO, WAV and HWDs for cluster 2 (cluster 3)

	SNAO	WAV	HWD
SNAO	1	− 0.69**	− 0.52** (0.30*)
WAV		1	0.40** (− 0.35*)
HWD			1

*Statistically significant at the 95% confidence level; **Statistically significant at the 99% confidence level

The spatial distribution of the GPH of cluster 3 (Fig. 5b) had a noticeably similar pattern to those of the Z-wave type heatwaves, as suggested by Yeo et al. (2019) (see also Fig. 5a in Yeo et al. 2019). They reported that the zonal wave propagates from the North Atlantic Ocean and across the Eurasian continent to East Asia, and the Z-wave type

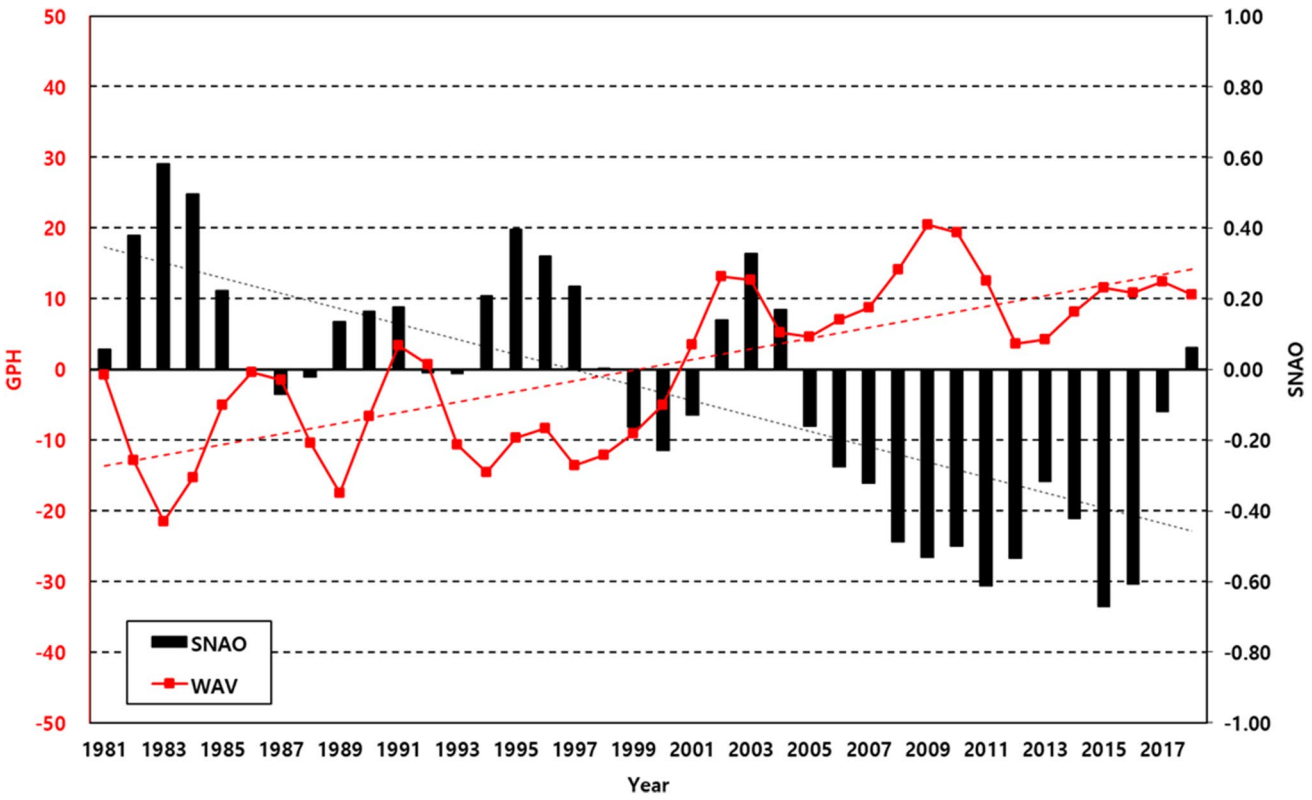

Fig. 6 Time series of the WAV and the SNAO during the midsummer (mid-July to mid-August). Dotted lines denote the regression lines

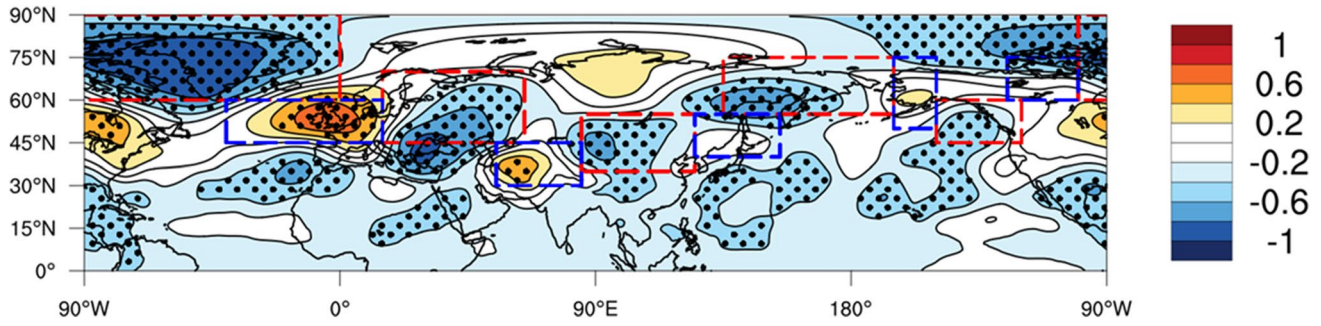

Fig. 7 The spatial distribution of the correlation coefficient relating an 8 year low-pass-filtered 500 hPa GPH during the midsummer (mid-July to mid-August) and SNAO. The statistically significant correlation coefficients at 99% confidence level are indicated by black dots. Rectangles with dashed lines are the same as those in Fig. 5c

heatwave was closely related to the positive NAO signal. Deng et al. (2019) reported that HWDs in northern China and the Yangtze River valley were likely to be associated with the Atlantic–Eurasian teleconnection with the presence of a wave generation mechanism related to the tropical North Atlantic Ocean SST anomaly. Notably, the regression pattern of the 500 hPa GPH and HWDs in northern China (see also Fig. 6 in Deng et al. 2019), corresponds to the large-scale pattern of cluster 2 in this study. This is significantly correlated with the summer NAO index. Indeed, previous studies have reported the relationship between the North Atlantic Ocean SST anomaly and summer NAO pattern in terms of the force and response (Wu et al. 2009; Lim and Seo 2019). A wave generation mechanism over the tropical North Atlantic Ocean, such as the forced warm SST anomaly, may vary the summer NAO teleconnection pattern, which is related to the Kamchatka blocking.

4 Summary and discussion

In this study, the long-term trend of the heatwave events in South Korea were investigated using cluster analysis. A total of 97 heatwave events from 1981 to 2018 were identified, and their synoptic patterns were categorized into three clusters using K-means cluster analysis. These consisted of distinctive spatial distributions of synoptic characteristics and TMAX for the three clusters, and atmospheric patterns such as Kamchatka blocking and the WNPSH, were associated with the heatwave characteristics. Cluster 2 had a large positive GPH anomaly over the Kamchatka Peninsula, while cluster 3 had a negative GPH anomaly. The HWDs of cluster 2 (cluster 3) from mid-July to mid-August had notably increased (decreased) in RECENT compared with the PAST. The long-term variabilities of large-scale patterns related to the synoptic pattern of both clusters were analyzed for the same period. The 500 hPa GPH had significantly increased in RECENT over the five representative regions in the Northern Hemisphere. This increasing pattern was spatially correlated with the large-scale pattern of clusters 2 and 3. The wave activity flux in both clusters indicated the propagation of the wave train along the five regions. We also examined the relationship between SNAO and GPH from mid-July to mid-August. The GPH was negatively and significantly correlated to the SNAO. The recent change in the long-term trend of HWDs over Korea may depend on variations in the large-scale atmospheric pattern in the Northern Hemisphere, which are correlated with the NAO index. In other words, as the summer NAO index has recently declined, it is possibly related to the increased (decreased) HWDs of cluster 2 (cluster 3) mediated by anomalous GPH over the Kamchatka Peninsula.

Although the HWDs of cluster 1 are not varying with decadal timescales, we found possible causes for its interannual variations Yeo et al. (2019). suggested that M-wave type heatwaves were driven by a northward propagating wave train from subtropical western North Pacific to East Asia. This is triggered by anomalous convective activity over the subtropical western North Pacific. East Asia Summer Monsoon (EASM) is known as a crucial component of convection over the subtropical western North Pacific (e.g., WNPSH), and it significantly influences extreme weather conditions in East Asia (Ha et al. 2012; Lee et al. 2013). The leading mode of EASM for 850 hPa wind introduced in Wu et al. (2008) was comparable to the composite M-type heatwave events map presented by Yeo et al. (2019). As such, there may be a correlation between the variability of the EASM index (EASMI) (Li and Zeng 2003) and the occurrence of M-type heatwave events. We tested the relationship between the EASMI in July–August and HWDs for each cluster, and there was a significant correlation coefficient (0.45) for cluster 1. The characteristics of the cluster 1-type heatwave is somewhat similar to the M-type heatwave.

Nevertheless, we presumed that cluster 1-type heatwave events also had the characteristics of the Z-wave type heatwave. For example, the spatial distribution of 500 hPa GPH

anomaly over western Europe had an opposite (similar) pattern to cluster 2 (cluster 3) (not shown). This implies that the cluster 1-type heatwave events may also be influenced by NAO forcing over this region, similar to clusters 2 and 3. It is possible that the wave train generated in this region may be combined by other forcings, such as the Indian monsoon (Ding and Wang 2007), Tibetan plateau (Kim et al. 2019), and subtropical western North Pacific (Liu et al. 2019). This study does not address this, and further studies on the dynamical mechanism and variability of cluster 1-type heatwave events are needed.

This study investigated the relationship between the summer NAO and HWD. However, a detailed description of the generating mechanism of the summer NAO-related wave train pattern is not included. Based on previous studies (Deng et al. 2019; Lim and Seo 2019), the SST over the tropical North Atlantic Ocean relating to the NAO in summer may be a source or trigger of the Atlantic–Eurasian wave patterns, which affect the HWDs covered in this study. There is a significant temporal correlation (0.32) between the HWDs of cluster 2 and the SST anomaly over the tropical North Atlantic Ocean (0–20° N, 30–60° W) (not shown). Further studies using numerical models are needed to examine the physical role of SST forcing over the tropical North Atlantic Ocean to the NAO and heatwaves over South Korea.

This study demonstrated that a greater number of cluster 2-type heatwave events, which is related to the strong blocking over the Kamchatka Peninsula, may occur with a decreasing summer NAO index trend. These results can provide important suggestions for predictability. The predictability of heatwave events in South Korea in a numerical weather prediction model may vary depending on the synoptic and large-scale circulation patterns. In particular, anomalous blocking events cannot be realistically captured by numerical models (Matsueda 2011). Thus, it is necessary to understand the mechanism of cluster 2-type heatwave events related to Kamchatka blocking for improving its predictability.

Acknowledgements This work was funded by the Korea Meteorological Administration Research and Development Program under grant KMIPA 2017-7010. This work was funded by the Ministry of Oceans and Fisheries, Korea project, entitled 'Investigation and Prediction System Development of Marine Heatwave around the Korean Peninsula originated from the Sub-Arctic and Western Pacific' (20190344). The ERA-Interim Project data were obtained freely from the CISL RDA (https://rda.ucar.edu/datasets/ds627.0/).

References

Barriopedro D, Fischer EM, Luterbacher J, Trigo RM, García-Herrera R (2011) The hot summer of 2010: redrawing the temperature record map of Europe. Science 332(6026):220–224

Choi J, An S-I, Yeh S-W, Yu J-Y (2013) ENSO-like and ENSO-induced tropical Pacific decadal variability in CGCMs. J Clim 26(5):1485–1501

Choi N, Lee MI, Cha DH, Lim YK, Kim KM (2020) Decadal changes in the interannual variability of heat waves in East Asia caused by atmospheric teleconnection changes. J Clim 33(4):1505–1522

Coumou D, Robinson A, Rahmstorf S (2013) Global increase in record-breaking monthly-mean temperatures. Clim Change 118(3–4):771–782

Coumou D, Di Capua G, Vavrus S, Wang L, Wang S (2018) The influence of Arctic amplification on mid-latitude summer circulation. Nat Commun 9(1):1–12

Dee DP, Uppala S, Simmons A, Berrisford P, Poli P, Kobayashi S, Andrae U, Balmaseda M, Balsamo G, Bauer DP (2011) The ERA-interim reanalysis: configuration and performance of the data assimilation system. Q J R Meteorol Soc 137(656):553–597

Deng K, Yang S, Ting M, Zhao P, Wang Z (2019) Dominant modes of China summer heat waves driven by global sea surface temperature and atmospheric internal variability. J Clim 32(12):3761–3775. https://doi.org/10.1175/jcli-d-18-0256.1

Ding Q, Wang B (2007) Intraseasonal teleconnection between the summer Eurasian wave train and the Indian monsoon. J Clim 20(15):3751–3767

Ding T, Qian W, Yan Z (2010) Changes in hot days and heat waves in China during 1961–2007. Int J Climatol 30(10):1452–1462

Fischer EM, Seneviratne SI, Vidale PL, Lüthi D, Schär C (2007) Soil moisture–atmosphere interactions during the 2003 European summer heat wave. J Clim 20(20):5081–5099

Folland CK, Knight J, Linderholm HW, Fereday D, Ineson S, Hurrell JW (2009) The summer North Atlantic Oscillation: past, present, and future. J Clim 22(5):1082–1103. https://doi.org/10.1175/2008jcli2459.1

Ha KJ, Heo KY, Lee SS, Yun KS, Jhun JG (2012) Variability in the East Asian monsoon: a review. Meteorol Appl 19(2):200–215

Hartigan JA, Wong MA (1979) Algorithm AS 136: a k-means clustering algorithm. J R Stat Soc Ser C Appl Stat 28(1):100–108

Hu L, Huang G (2020) The changes of high-temperature extremes and their links with atmospheric circulation over the Northern Hemisphere. Theor Appl Climatol 139(1–2):261–274

IPCC (2013) In: Stocker TF et al (eds) Climate change 2013: the physical science basis. Contribution of working group I to the fifth assessment report of the intergovernmental panel on climate change. Cambridge University Press, Cambridge, p 1535

Jian-Qi S (2012) Possible impact of the summer North Atlantic Oscillation on extreme hot events in China. Atmos Ocean Sci Lett 5(3):231–234

Kim D-W, Deo RC, Chung J-H, Lee J-S (2015) Projection of heat wave mortality related to climate change in Korea. Nat Hazards 80(1):623–637. https://doi.org/10.1007/s11069-015-1987-0

Kim MK, Oh JS, Park CK, Min SK, Boo KO, Kim JH (2019) Possible impact of the diabatic heating over the Indian subcontinent on heat waves in South Korea. Int J Climatol 39(3):1166–1180

Kornhuber K, Coumou D, Vogel E, Lesk C, Donges JF, Lehmann J, Horton RM (2020) Amplified Rossby waves enhance risk of concurrent heatwaves in major breadbasket regions. Nat Clim Change 10(1):48–53

Krzanowski WJ, Lai YT (1988) A criterion for determining the number of groups in a data set using sum-of-squares clustering. Biometrics 44(1):23–34

Kysely J, Kim J (2009) Mortality during heat waves in South Korea, 1991 to 2005: how exceptional was the 1994 heat wave? Clim Res 38:105–116. https://doi.org/10.3354/cr00775

Lee W-S, Lee M-I (2016) Interannual variability of heat waves in South Korea and their connection with large-scale atmospheric circulation patterns. Int J Climatol 36(15):4815–4830. https://doi.org/10.1002/joc.4671

Lee S-S, Seo Y-W, Ha K-J, Jhun J-G (2013) Impact of the western North Pacific subtropical high on the East Asian monsoon precipitation and the Indian Ocean precipitation in the boreal summertime. Asia Pac J Atmos Sci 49(2):171–182

Li JP, Zeng QC (2003) A new monsoon index and the geographical distribution of the global monsoons. Adv Atmos Sci 20(2):299–302

Li M, Yao Y, Luo D, Zhong L (2019) The linkage of the large-scale circulation pattern to a long-lived heatwave over Mideastern China in 2018. Atmosphere 10(2):89

Lim W-I, Seo K-H (2019) Physical-statistical model for summer extreme temperature events over South Korea. J Clim 32(6):1725–1742. https://doi.org/10.1175/jcli-d-18-0201.1

Liu Q, Zhou T, Mao H, Fu C (2019) Decadal variations in the relationship between the western pacific subtropical high and summer heat waves in East China. J Clim 32(5):1627–1640

Luterbacher J, Dietrich D, Xoplaki E, Grosjean M, Wanner H (2004) European seasonal and annual temperature variability, trends, and extremes since 1500. Science 303(5663):1499–1503. https://doi.org/10.1126/science.1093877

Matsueda M (2011) Predictability of Euro-Russian blocking in summer of 2010. Geophys Res Lett 38:L06801. https://doi.org/10.1029/2010GL046557

Meehl GA, Tebaldi C (2004) More intense, more frequent, and longer lasting heat waves in the 21st century. Science 305(5686):994–997

Min KH, Chung CH, Bae JH, Cha DH (2019) Synoptic characteristics of extreme heatwaves over the Korean Peninsula based on ERA Interim reanalysis data. Int J Climatol. https://doi.org/10.1002/joc.6390

Min S-K, Kim Y-H, Lee S-M, Sparrow S, Li S, Lott FC, Stott PA (2020) Quantifying human impact on the 2018 summer longest heat wave in South Korea. Bull Am Meteorol Soc 101(1):S103–S108

Nakai S, Itoh T, Morimoto T (1999) Deaths from heat-stroke in Japan: 1968–1994. Int J Biometeorol 43(3):124–127

Ren F, Cui D, Gong Z, Wang Y, Zou X, Li Y, Wang S, Wang X (2012) An objective identification technique for regional extreme events. J Clim 25(20):7015–7027

Stefanon M, D'Andrea F, Drobinski P (2012) Heatwave classification over Europe and the Mediterranean region. Environ Res Lett 7(1):014023. https://doi.org/10.1088/1748-9326/7/1/014023

Sun Y, Zhang X, Zwiers FW, Song L, Wan H, Hu T, Yin H, Ren G (2014) Rapid increase in the risk of extreme summer heat in Eastern China. Nat Clim Change 4(12):1082–1085. https://doi.org/10.1038/nclimate2410

Takaya K, Nakamura H (2001) A formulation of a phase-independent wave-activity flux for stationary and migratory quasigeostrophic eddies on a zonally varying basic flow. J Atmos Sci 58(6):608–627

Thompson DW, Wallace JM (1998) The Arctic Oscillation signature in the wintertime geopotential height and temperature fields. Geophys Res Lett 25(9):1297–1300

Wang SY, Davies RE, Gillies RR (2013) Identification of extreme precipitation threat across midlatitude regions based on short-wave circulations. J Geophys Res Atmos 118(19):11059–11074

Wang P, Tang J, Wang S, Dong X, Fang J (2017) Regional heatwaves in china: a cluster analysis. Clim Dyn 50(5–6):1901–1917. https://doi.org/10.1007/s00382-017-3728-4

Wang SSY, Kim H, Coumou D, Yoon JH, Zhao L, Gillies RR (2019) Consecutive extreme flooding and heat wave in Japan: are they becoming a norm? Atmos Sci Lett 20(10):e933

Ward R (1925) The climates of the United States. American Meteorological Society, The AMS Glossary of Meteorology, pp 383–395. http://glossary.ametsoc.org/wiki/Heat_wave

Wu B, Zhang R, Ding Y, D'Arrigo R (2008) Distinct modes of the East Asian summer monsoon. J Clim 21(5):1122–1138

Wu Z, Wang B, Li J, Jin F-F (2009) An empirical seasonal prediction model of the East Asian summer monsoon using ENSO and NAO. J Geophys Res Atmos 114:D18120. https://doi.org/10.1029/2009JD011733

Yeh S-W, Won Y-J, Hong J-S, Lee K-J, Kwon M, Seo K-H, Ham Y-G (2018) The record-breaking heat wave in 2016 over South Korea and its physical mechanism. Mon Weather Rev 146(5):1463–1474. https://doi.org/10.1175/mwr-d-17-0205.1

Yeo SR, Yeh SW, Lee WS (2019) Two types of heat wave in Korea associated with atmospheric circulation pattern. J Geophys Res Atmos. https://doi.org/10.1029/2018jd030170

Yoon D, Cha DH, Lee G, Park C, Lee MI, Min KH (2018) Impacts of synoptic and local factors on heat wave events over southeastern region of Korea in 2015. J Geophys Res Atmos 123(21):12081–12096